WATER RESOURCES RESEARCH, VOL. 37, NO. 5, PAGES 1221–1229, MAY 2001

# Monitoring pumping test response in a fractured aquifer using ground-penetrating radar

Georgios P. Tsoflias,[1] Todd Halihan,[2] and John M. Sharp Jr.
Department of Geological Sciences, The University of Texas at Austin, Austin, Texas

**Abstract.** Fractured aquifers present a number of problems when attempting to characterize flow on the well scale (less than 100 m). Standard hydraulic testing methods are expensive because of the need for installation of monitoring wells. Geophysical methods may suffer from a lack of resolution and nonunique solutions to data interpretation. We used ground-penetrating radar (GPR) surveying during a pumping test in a well-characterized, fractured, carbonate aquifer to monitor the response of a permeable subhorizontal fracture plane. We observed radar signal amplitude and waveform variations along a fracture reflector and correlated the radar signal response to changes in the water saturation of the fracture. Combining hydraulic measurements with GPR data and electromagnetic modeling, we identified an asymmetric fracture drainage pattern, provided accurate spatial information about the saturation of the fracture, and detected the presence of hydraulic boundaries. This study demonstrates that GPR surveying can be used successfully for real-time monitoring of pumping tests in fractured carbonate aquifers.

## 1. Introduction

Ground-penetrating radar (GPR) is a remote sensing, noninvasive, high-frequency electromagnetic method that has been successfully employed to investigate the near surface for a variety of applications [*Davis and Annan*, 1989; *Mellett*, 1995]. In clastic aquifers, GPR has been used to characterize near-surface hydrogeologic properties [*Beres and Haeni*, 1991], to monitor migration of contaminants [*Brewster and Annan*, 1994], to identify water content variations [*Greaves et al.*, 1996] and fluid flow paths [*Birken and Versteeg*, 1998], and to locate the water table [*van Overmeeren*, 1998]. In low-electrical-conductivity environments, GPR provides high-resolution imaging of the subsurface of the order of centimeters to decimeters and depth of investigation of several meters. Under appropriate conditions these capabilities make GPR a suitable technique for the study of fractured carbonate aquifers and the identification of groundwater flow paths [*Dubois*, 1995; *Tsoflias and Sharp*, 1998].

Flow and transport in fractured rock aquifers is dominated by the heterogeneous nature of these aquifers. Standard hydraulic testing is limited by assumptions that must be made to interpret test data. Even with rigorous testing programs, it is difficult to characterize fractured aquifers adequately. Although packer tests can be useful for determining small-scale hydraulic properties, interpretation can be complicated by multiple fractures in a single test interval, nonconductive fractures, or variations in the fracture plane [*Geier et al.*, 1995]. Since measurement is limited to one location, no information is provided about how the tested fractures may interconnect away from the borehole. Thus the response may measure some network property, instead of that of a single fracture or zone [*Geier et al.*, 1995]. Recent work in monitoring pumping tests in unconfined, clastic aquifers using GPR successfully identified the transition zone between the residually saturated portion of the aquifer and the water-saturated capillary fringe [*Endres et al.*, 1997, 2000]. We are not aware of any previous monitoring of pumping tests in fractured aquifers using GPR.

In the investigation described in this paper, we acquired GPR reflection data during a pumping test in a fractured carbonate aquifer to determine if changes in fracture saturation could be observed remotely and in real time. We employed forward electromagnetic modeling of thin layers to investigate radar waveform changes produced by changes in fracture saturation. We correlated the modeled responses of thin layers to the GPR data and interpreted the fracture drainage pattern produced by the pumping test. Our results show that GPR surveying can overcome some of the limitations of conventional hydraulic testing of fractured aquifers.

## 2. Site Description

GPR surveys were conducted at the Bissen Quarry hydrogeologic test site, located approximately 7 km (4.5 miles) southwest of Sturgeon Bay, Wisconsin, United States of America (Figure 1). The test site consists of the fractured Silurian Byron Dolomite, which has been quarried exposing a clean horizontal survey surface. The site is part of a regional aquifer along the western flank of the Michigan Basin. Recharge occurs through vertical fractures, and rapid lateral flow occurs through regionally continuous horizontal high-permeability zones [*Bradbury and Muldoon*, 1992; *Muldoon and Bradbury*, 1996; *Tsoflias and Sharp*, 1998].

At Bissen Quarry the Wisconsin Geological and Natural History Survey (WGNHS) has conducted intensive hydrogeologic studies on an approximately 40 m × 25 m surface of exposed dolomite to characterize and model flow through the fractured aquifer. Nineteen wells were installed at an approx-

[1]Now at Minerals Management Service, U.S. Department of the Interior, New Orleans, Louisiana.
[2]Now at School of Geology, Oklahoma State University, Stillwater, Oklahoma.



Paper number 2000WR900297.
0043-1397/01/2000WR900297$09.00

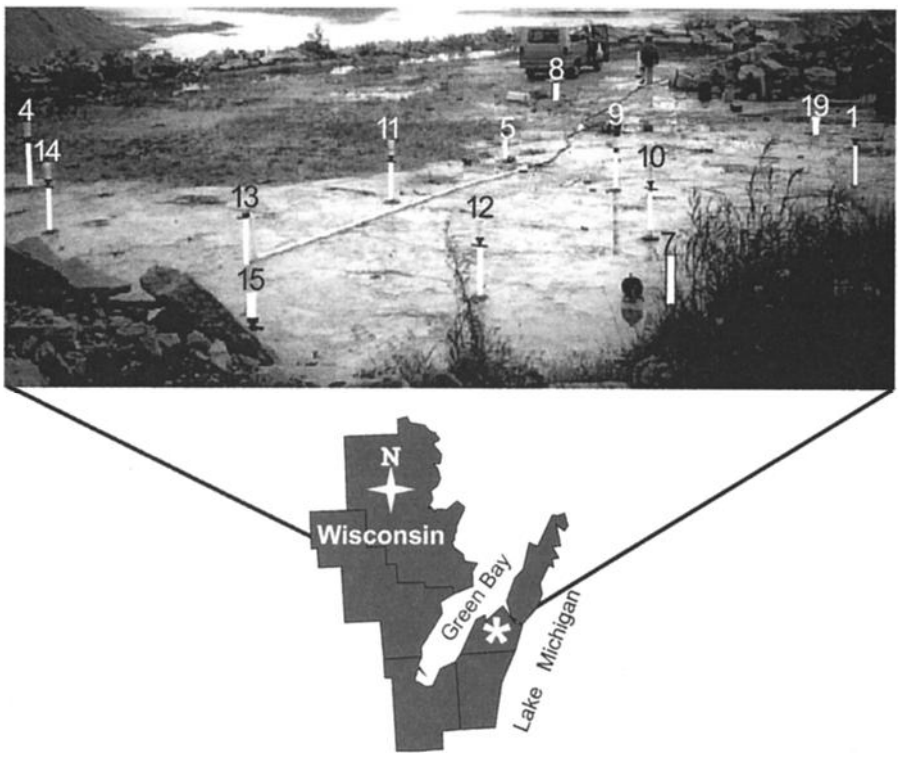


**Figure 1.** Photo of Bissen Quarry site and map of regional location in Door County, Wisconsin, United States of America. Pumping well 13 shown with PVC casing and PVC piping to surface pump located away from ground-penetrating radar (GPR) survey location. PVC was used to prevent electromagnetic interference during surveying. The water table is very shallow as indicated by the flooded quarry pits at the top of Figure 1.

imate 3-m spacing grid; most of the wells are 11 m in depth (Figure 1). Site hydrogeology was characterized using a series of hydraulic tests, borehole logs, stratigraphic analysis of cores, outcrop studies, surface mapping of vertical fractures, and GPR surveys. These studies identified four major horizontal bedding plane fractures (f1 at 1.35 m, f2 at 4.25 m, f3 at 6.4 m, and f4 at 12 m below surface), two dissolution zones (d1 at 2.72 m and d2 at 7.45 m below surface), a diagenetic zone (z1 at 3.35 m below surface), and an orthogonal set of subvertical fractures (N75°E and N25°W). Hydraulic conductivity data show a bimodal distribution ranging through 7 orders of magnitude, indicating high-conductivity fractures and low-conductivity rock matrix [*Muldoon and Bradbury*, 1996]. WGNHS studies showed that lithologies and horizontal stratigraphic discontinuities control both the aquifer storage capacity and the distribution of preferential flow paths. Preferential flow zones formed along bedding planes, diagenetic surfaces, and cycle sequence boundaries. These flow zones have been further enhanced by dissolution.

We selected the Bissen Quarry site for this study because (1) it is an important fractured aquifer for the region with a low-porosity, low-permeability matrix and hydraulically conductive discontinuities, (2) there is a large hydrogeologic database available from WGNHS studies, and (3) low-electrical-conductivity geologic formations and low-electromagnetic ambient noise environments allow the acquisition of good quality, high resolution GPR data [*Tsoflias and Sharp*, 1998].

## 3. Methods

In order to test if GPR surveying could image real-time water saturation changes along flow paths, we collected radar data and measured hydraulic heads both before and during a pumping test. Modeling of radar and hydraulic data allowed us to integrate and interpret the information available from both data sources.

### 3.1. Data Collection and Processing

Two GPR surveys were conducted in this investigation. We acquired the first radar survey in August 1997, under undisturbed hydrologic conditions, as a pseudo-three-dimensional (3-D) data volume (closely spaced parallel two-dimensional (2-D) profiles) covering a 11 m × 10 m surface area on a 0.1-m-square grid. The second survey, collected in June 1998 during a pumping test, consisted of four 2-D reflection profiles acquired in a radial pattern centered about the pumping well (well 13) and a single profile south of the pumping well (Figure 2). We acquired both GPR surveys using a Pulse EKKO 100 system (Sensors and Software, Inc., Mississauga, Ontario, Canada), with a 400-V transmitter, 200-MHz center frequency antennas, 0.1-m station (trace) spacing, 64 trace stacks, a 600-ns record length, and a 0.8-ns sampling interval. Transmitter-receiver antenna separation (offset) was 1.5 m for the 3-D data and 0.5 m for the 2-D lines. We selected different antenna offsets because of the different objectives of the surveys. The

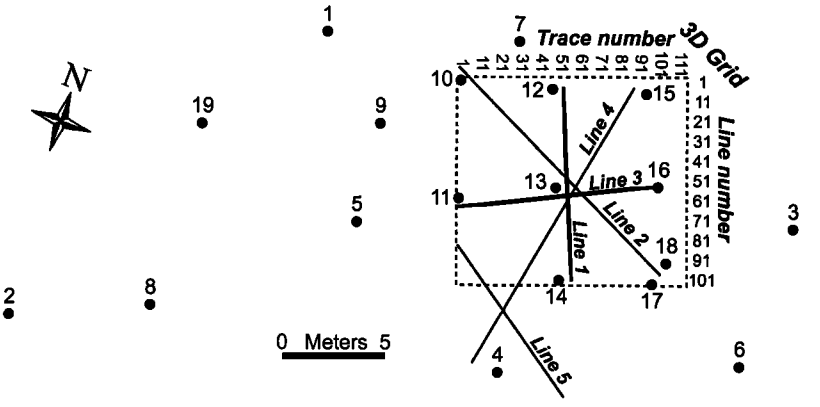


**Figure 2.** Site map illustrating the well locations (circles), two-dimensional (2-D) GPR lines (solid lines) acquired during a pumping test at well 13, and three-dimensional (3-D) grid coverage (dashed outline) acquired under undisturbed hydrologic conditions.

1997 3-D data were aimed at optimum imaging of shallow and deep sections of the aquifer. The 1998 2-D data were aimed at shallow imaging of water table changes produced by the pumping test at well 13.

We applied minimal processing to the GPR data in order to preserve the relative amplitude, frequency, and phase of the signal. Processing of both 2-D and 3-D surveys consisted of (1) debias, high-pass-frequency filtering designed by Sensors and Software to remove low-frequency noise induced from one antenna to another; (2) trace leveling (flattening) of the corresponding constant antenna offset direct airwave arrival to correct for instrumentation time drifts; (3) trace bulk time shifting to the corresponding time zero, defined as the time the transmitter began transmitting; and (4) amplitude gaining, using a $[\text{time}]^2$ factor to compensate for the exponential signal amplitude decay while preserving relative amplitude information (i.e., amplitude variations) along horizontal reflectors [*Tsoflias*, 1999].

The GPR surveys imaged coherent reflectors to 240-ns two-way travel time (approximately 12 m depth at an average velocity of 0.1 m $ns^{-1}$). For comparison, two GPR profiles are displayed over the same location near wells 12, 13, and 14 (Figure 3). The 2-D line 1 was acquired in 1998 during the pumping test at well 13 with the water table near the survey floor (less that 0.5-m depth below surface, approximately 10 ns). The 3-D inline 53 was acquired in 1997 under undisturbed hydrologic conditions at which time the water table was at 2-m depth (approximately 40 ns). Depth to the water table was monitored at observation wells.

The pumping test for the study was conducted as an open borehole test with observation wells. To minimize the introduction of electromagnetic noise to the GPR data, there was no metal piping in the borehole and the pump was placed approximately 20 m away from the pumping well by laying PVC pipe on the quarry floor (Figure 1). The well casings on the site were primarily PVC, but a few wells outside the survey area had metal casings. The head levels were monitored at 13 piezometers and two open boreholes before and after the GPR survey (Figure 4). Water level was continuously monitored using a pressure transducer and data logger (Hermit 2000, In-Situ Corp., Laramie, Wyoming) in the upper section of well 19, the only deep well at the site (Figure 2). Well 19 had a packer installed at a depth of 11 m to allow the pumping test to be correlated with previous tests that occurred prior to the installation of the deep well. Water level was not monitored in the pumping well during the survey because no space was available between the pump piping and the well casing. The pumping rate for the test was 3.2 L $s^{-1}$ (50 gpm), measured using a 20-gal. barrel and a stopwatch.

The pumping test had been planned to coincide with dry weather and the rental of commercial GPR equipment. However, intense overnight thunderstorms interrupted the pumping test and raised water levels to the highest ever observed for the site. The GPR survey was conducted the following day during a rain-free period, when the drawdown was at approximate steady state conditions and the survey area (exposed dolomite quarry floor) was free of ponded water. During GPR data acquisition we measured less than 0.01-m change in head levels, with an average change of 0.005 m, some of which is attributed to water level measurement errors.

### 3.2. Data Analysis and Modeling

In low-electrical-conductivity media, such as carbonates and freshwater, the amplitude of a radar reflection at a single planar interface is controlled by the electromagnetic velocity contrast (a function of dielectric constant contrast) across the interface, the angle of incidence, and the polarization of the wave field [*Straton*, 1941]. For a thin layer between two interfaces, such as a fracture or a dissolution-enhanced flow path, the reflection strength is also a function of layer thickness and signal frequency. Figure 5 shows a plot of reflection coefficient versus layer thickness for an analytical model with the dielectric properties of the Byron Dolomite and a 200-MHz radar signal [*Tsoflias*, 1999].

We employed 2-D finite difference time domain electromagnetic modeling [*Poot*, 1998] to simulate the effects of water saturation changes in a horizontal thin layer (subresolution thickness) to GPR signal response. Model parameters simulated a horizontally stratified dolomite environment with appropriate electromagnetic wave velocity of propagation ($v$) and conductivity ($\sigma$) for the field site and the same field data acquisition geometry (antenna offset and fracture depth). We determined unsaturated and saturated dolomite electromagnetic (EM) wave velocities of 0.11 m $ns^{-1}$ and 0.08 m $ns^{-1}$, respectively, using velocity analysis of four multioffset common midpoint (CMP) surveys [*Taner and Koehler*, 1969]. Electrical conductivities were estimated to be 0.7 mS $m^{-1}$ for the unsaturated and 1.0 mS $m^{-1}$ for the shallow saturated portion of the

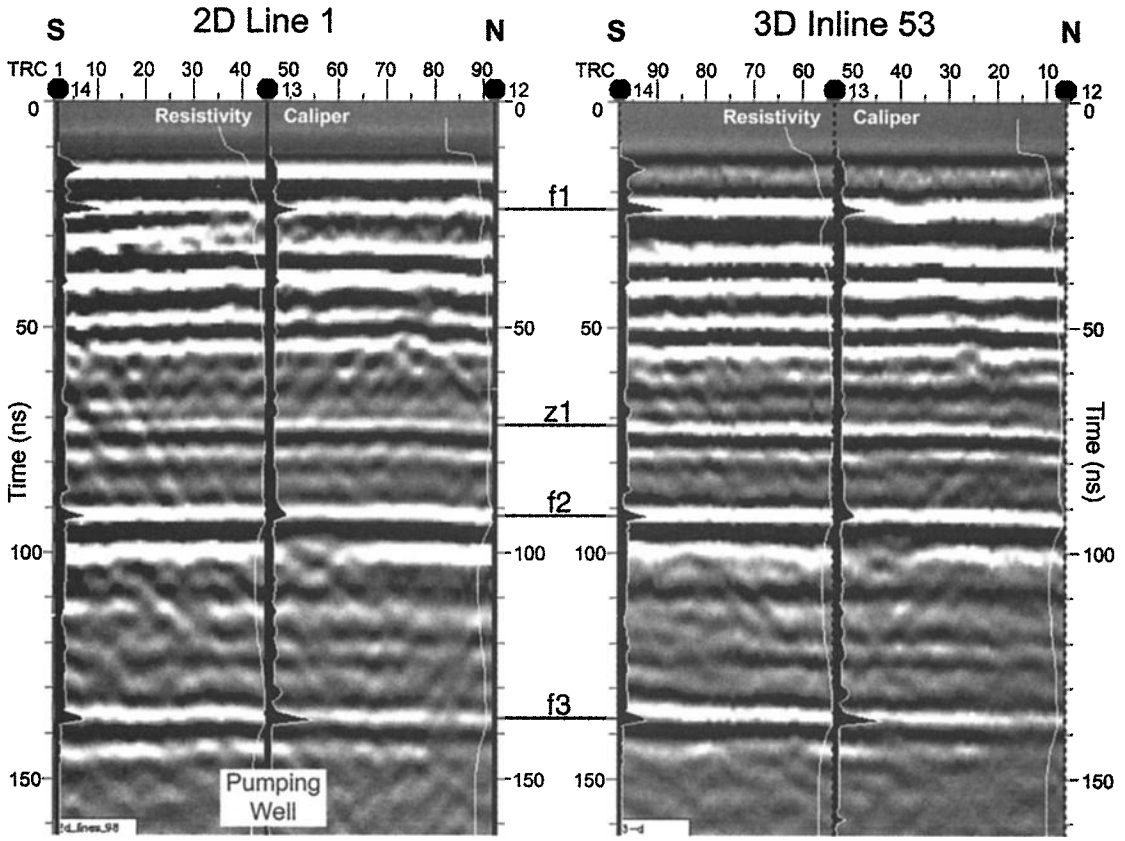


**Figure 3.** GPR profiles displaying the same section through wells 12, 13, and 14. Trace numbers (TRC) and well surface locations (circles) are identified on each profile. Caliper and resistivity log curves are displayed along the well bores. On the left is the 1998 2-D line 1 collected during a pumping test at well 13. On the right is the 1997 3-D inline 53 collected under undisturbed hydrologic conditions. Continuous strong radar reflectors correspond to known flow paths (horizontal discontinuities f1, f2, and f3 and dissolution zone z1).

aquifer based on published ranges for carbonates [*Davis and Annan*, 1989] and the low permeability of the rock matrix. Electrical conductivity variation of 1 order of magnitude did not yield significant changes in the modeling of shallow interfaces; thus the values selected for the model are considered adequate. The horizontal fracture was under three conditions: (1) air filled; (2) freshwater saturated; and (3) partially saturated with an upper air-filled layer and a lower water-filled layer. The EM parameters of air and freshwater are (1) air $\sigma$ = 0 mS m$^{-1}$ and $v$ = 0.3 m ns$^{-1}$; and freshwater $\sigma$ = 1.0 mS m$^{-1}$, and $v$ = 0.033 m ns$^{-1}$ [*Davis and Annan*, 1989]. The model employed a 1-cm grid size in two dimensions, a 0.01-ns time step, a 200-MHz Gaussian source pulse (wavelet), and a thin horizontal layer thickness of 2 cm.

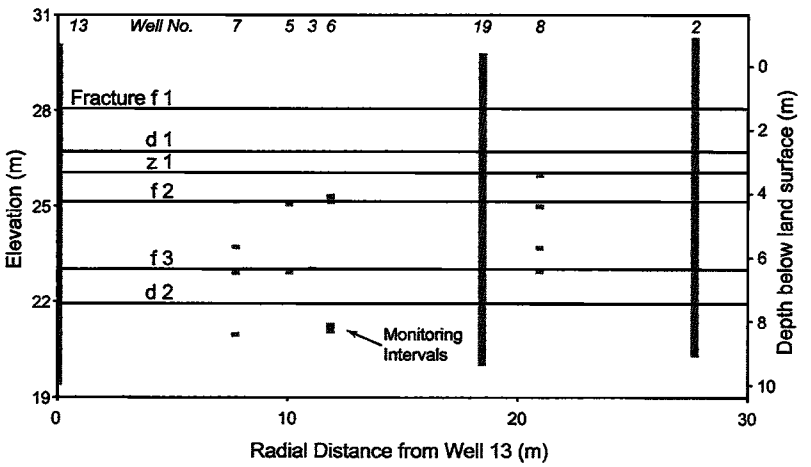


**Figure 4.** Hydraulic head monitoring points at the Bissen quarry including open boreholes and piezometers. No observation data are available from piezometers monitoring fracture f1 and dissolution zone d1.

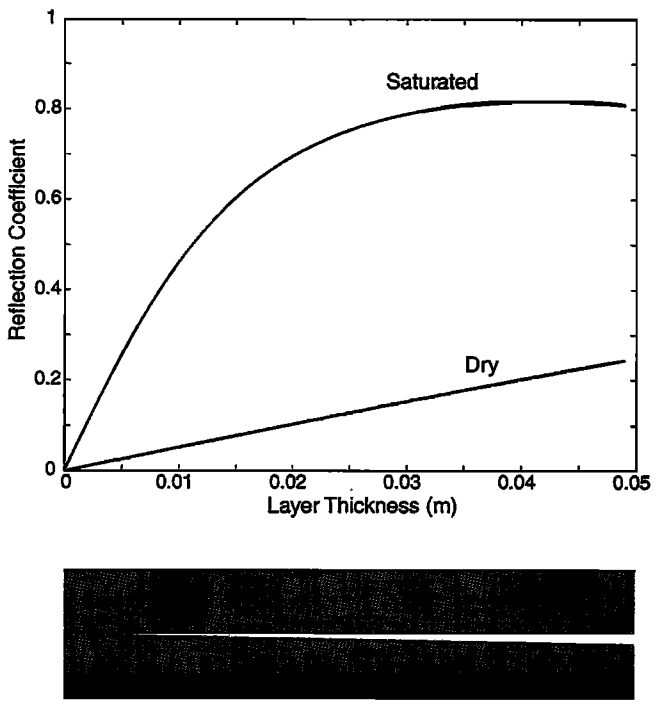


**Figure 5.** Plot of reflection coefficient versus layer thickness for a 200-MHz normal incident plane wave to a saturated and unsaturated thin layer of varying thickness contained within a rock matrix with the dielectric properties of the Byron Dolomite [*Tsoflias*, 1999].

The pumping test analysis used the *Neuman* [1975] type-curve method for an unconfined aquifer to obtain an estimate of transmissivity. Because of possible well bore storage effects, variations in pump speed, and thunderstorms in the early portion of the pumping test, the recovery segment (1375–2660 min on Figure 6) of the test was used for analysis of the drawdown data. Using these data, two steady state models for the observed water level elevations in the system (at about 1300 min on Figure 6) were utilized to determine which horizontal fractures drained during the GPR survey. A confined infinite aquifer model and an unconfined model, which assumed that the drainage ditch at the site acted as a hydraulic boundary 22 m from the pumping well, were used [*Thiem*, 1906; *Fetter*, 1994, p. 215]. We combined these models with head observations to determine (1) which horizontal fracture planes at the site were drained during the test and (2) the radius of fracture draining.

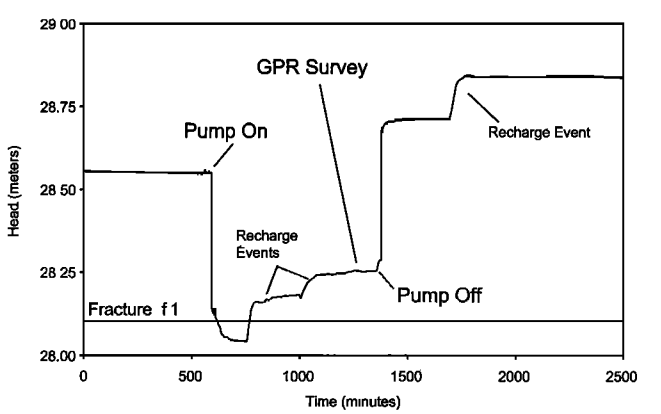


**Figure 6.** Water levels in open borehole 19 during pumping test. The water level early in the pumping test drained below fracture 1, but subsequent precipitation caused the water level to rise above fracture 1 in well 19.

## 4. Results

First, the 2-D GPR pumping test survey was compared with the 3-D undisturbed water table survey for reflector similarities and differences. We then examined the predicted signal responses from forward EM modeling and used them to interpret the 2-D lines. Finally, we used the hydraulic-test analysis to determine the validity of the GPR interpretation.

### 4.1. GPR

GPR profiles acquired over the same location prior to and during the pumping test are shown in Figure 3. Both radar profiles display the same subsurface features consisting of horizontally layered carbonate facies and horizontal discontinuities (fractures and a diagenetic zone). Caliper log maximum and resistivity log minimum deflections displayed along the wells identify the locations of known horizontal fractures f1 (1.35-m depth), f2 (4.25 m), and f3 (6.4 m) [*Muldoon and Bradbury*, 1996]. Well cores identified diagenetic zone z1 (3.35 m) [*Muldoon and Bradbury*, 1996]. These high-hydraulic-conductivity flow paths correlate to increased amplitude continuous radar reflectors at 24-, 75-, 92-, and 137-ns two-way travel time (Figure 3). Below 35 ns, the two profiles are nearly identical and exhibit small amplitude differences that are attributed to different antenna offset, different electromagnetic wave field orientation, different water table depth, and the use of different radar systems (although of the same model). Small vertical time shifts of horizontal reflectors between the two profiles (up to 3-ns delay observed in the shallow section on 3-D inline 53) are caused by the different antenna offsets and associated reflection travel paths not compensated for in processing. These effects decrease with depth as travel paths approach normal incidence to reflecting interfaces. Additionally, small velocity differences produced by different water table depths contribute to minor reflector time shifting at this low-porosity site. Note that the top of the saturated zone does not yield a radar reflection, although velocity analysis of CMP surveys indicated velocities of 0.11 m $ns^{-1}$ and 0.08 m $ns^{-1}$ for the shallow (unsaturated) and deeper (saturated) sections of the aquifer, respectively. The lack of a reflector is due to the lack of a sharp dielectric constant contrast at the unsaturated-saturated interface in the low-porosity dolomite matrix. It is the secondary porosity features (fractures and the diagenetic zone) that give rise to strong reflectors. At the level of the shallowest horizontal fracture (24 ns), significant differences are observed in the two profiles (Figure 3). The 3-D profile shows no substantial lateral variation along the length of fracture f1. The 2-D profile shows amplitude variations along the length of the fracture reflector (24–30 ns), with the strongest amplitudes to the south of the profile and the weakest amplitudes at the pumping well. Although reflector amplitude values cannot be compared directly between the 2-D and 3-D profiles, the reflector variability in each profile can be used to identify differences between the two profiles. The difference between the shallow sections of the two profiles (pumping test versus undisturbed) shows that the pumping test introduced changes in the electromagnetic properties of the aquifer at the 24-ns region. We interpret these changes as the result of changes in

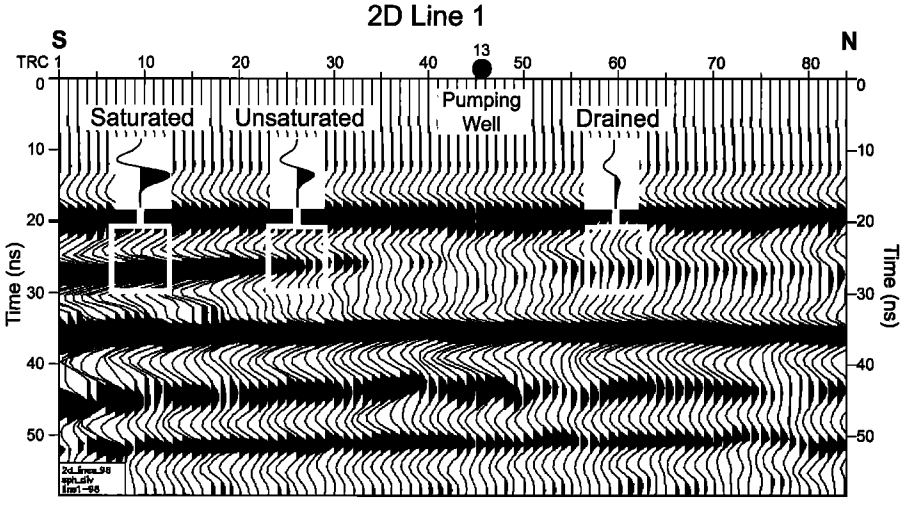


**Figure 7.** The 2-D line 1 during pumping test at well 13. Single trace inserts of the modeled waveforms for saturated, unsaturated (also referred as partially saturated), and drained fracture models are shown along with the corresponding recorded waveforms outlined by open boxes. Refer to text for detailed analysis.

the water saturation of horizontal fracture f1. Furthermore, the observed waveform changes are not symmetric about the pumping well 13. This suggests that the drainage area of this shallow horizontal flow path is not concentric about the pumping well. Similar amplitude patterns (i.e., high amplitudes to the south, lowest amplitudes at the pumping well, and intermediate amplitudes to the north) were observed in all four 2-D radial lines collected during the pumping test.

Analytical computations of the magnitude of reflection coefficients, for saturated and dry layers of varying thickness enclosed in dolomite matrix, indicate that significantly stronger amplitude reflections result from a water-saturated layer (Figure 5) [*Tsoflias*, 1999]. Two-dimensional finite difference modeling of radar signal response shows that the strongest amplitude corresponds to a fully saturated fracture and an intermediate amplitude response corresponds to a partially saturated fracture (Figure 7 inserts). A drained fracture yields the lowest amplitude response and an apparent delay in time and stretching of the waveform, as a result of the reversal of reflectivity and the decreased sharpness of the reflective interface compared to the saturated model. Note that because of uncertainty in the model parameters (rock matrix and interstitial water electrical conductivities, complex dielectric constants, velocities of propagation, time-variant frequency content, roughness of the interfaces, and fracture aperture), the modeling is used to assist interpretation rather than for a precise simulation of field conditions.

Inspection of 2-D line 1 (Figure 7) in the 24- to 28-ns time interval (trough-peak) along the fracture reflection shows the strongest amplitudes to the south of the section (traces 1–20). Intermediate amplitudes are observed south of the pumping well (traces 21–33) decreasing to minimum amplitudes around the pumping well (traces 42–48). Small-amplitude levels and stretched waveforms are observed north of well 13. According to modeling results the strong amplitudes to the south of the radar line (traces 1–20) indicate fully saturated sections along the fracture. The intermediate amplitudes showing a decreasing trend toward the pumping well (traces 21–33) indicate partially saturated areas along the fracture with decreasing water saturation when approaching well 13. Closest to the pumping well 13 (traces 42–48), where the fracture is expected to be drained, the observed radar waveform has the lowest amplitude and is stretched and delayed in time, similar to the waveform predicted by modeling. North of the pumping well, signal amplitudes remain at low levels, and waveforms appear delayed in time and stretched compared to saturated and partially saturated waveforms. These are also interpreted as responses from nearly drained sections of the fracture. Similar amplitude and waveform variations are present in all four 2-D radial lines.

When the above observations are correlated along all of the 2-D survey lines, an interpreted drainage pattern for the horizontal fracture f1 can be developed. The 2-D (pumping test) data show significant amplitude variation (0–430 $\mu$V) at the 28-ns peak reflector for all 2-D lines around the pumping well, compared to the clearly smaller-amplitude variation (80–160 $\mu$V) along 3-D inline 53 (undisturbed) (Plate 1). High and intermediate amplitudes are consistently south of the pumping well, and low amplitudes are centered on well 13 and extend to the north. Waveform interpretation yields the contoured drainage pattern for the fracture (Plate 1). The low to intermediate amplitude transition at the northwestern end of line 2 is used as the northernmost control point of the drained area contour. Note that drainage of the horizontal fracture is not symmetric about the pumping well and indicates a recharge boundary from the south. This drainage pattern agrees with the setting of the field site where a drainage ditch, located to the south of the pumping well, provided rapid recharge of the shallow horizontal fracture.

### 4.2. Hydraulic Data

The monitoring data at well 19 (Figure 6) indicated that the hydraulic head at the site was below the level of the uppermost fracture during the early portion of the pumping test. Subsequent recharge raised water levels at well 19 above the level of the fracture. Examining all available head data indicated that the head distribution on the site was very complex, as expected in a heterogeneous fractured aquifer.

The pumping test transmissivity of $2.5 \times 10^{-3}$ m$^2$ s$^{-1}$ is in close agreement with tests conducted on the site at other

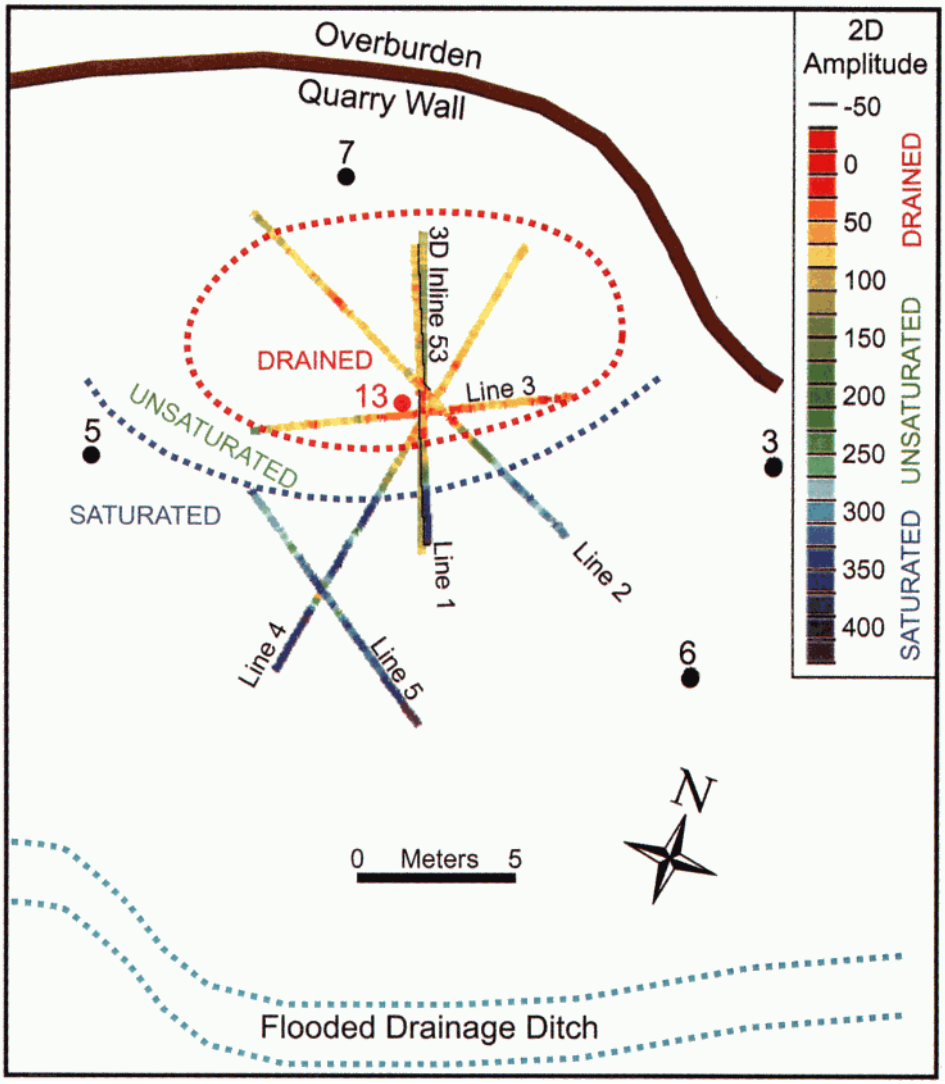


**Plate 1.** Amplitude of the 28-ns peak along the 2-D GPR data during the pumping test at well 13 and the 3-D inline 53 prior to the pumping test. Contour lines indicate drainage pattern interpretation for the shallowest fracture reflector. Well locations are given to compare with Figure 2. Amplitude legend corresponds to 2-D profiles collected under pumping conditions. The 3-D inline 53 is given to illustrate the lack of amplitude variability in the prepumping test data.

boreholes [*Muldoon and Bradbury*, 1998]. The steady state models indicate that fracture f1 is drained to a maximum radius of 16 m and a minimum radius of 6 m (Figure 8). Without head data closer to the borehole in the individual fracture the radius of fracture draining cannot be determined with greater accuracy.

## 5. Discussion

GPR surveying identified real-time drainage of a horizontal fracture during a pumping test, even though the hydrologic conditions were not satisfactory for traditional test analysis. We infer that with higher pumping rates and no concurrent recharge, we could have monitored drainage of deeper horizontal fractures with GPR surveying. Use of the real-time and three-dimensional capabilities of GPR along with pumping and packer tests can improve our understanding of fractured aquifer flow properties at the well scale. This technique has better chances of monitoring water saturation changes in fractures than in a low-porosity rock matrix. Porous rock matrix would require prolonged pumping in order to drain sufficient moisture from the pore space to generate dielectric constant contrasts detectable by surface GPR systems. At Bissen Quarry the lack of a water table reflector under undisturbed hydrologic conditions suggests that even prolonged pumping might not generate detectable dielectric constant contrasts in the dolomite matrix.

Reflected GPR signal amplitude variations of up to 70% can be introduced by changes in the aperture of a fracture (0–2 cm), as shown in Figure 5 [*Tsoflias*, 1999]. Thus, in order to correlate radar signal amplitude and waveform variations to water saturation changes due to a pumping test, radar data must be obtained prior to the test and used as a baseline for comparison. It should be noted that, in this study, a direct comparison of amplitudes between the two surveys is not valid (i.e., subtracting one data set from the other to identify the differences) because different antenna offsets affect both am-

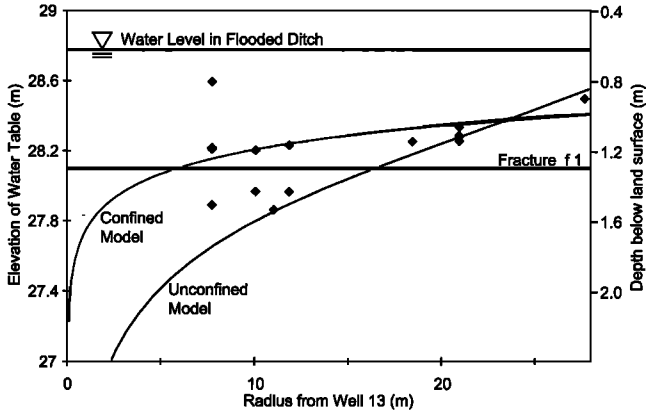


**Figure 8.** Water elevations during GPR surveying and steady state models for confined and unconfined conditions. The diamonds represent water levels obtained from the piezometers shown in Figure 4. The elevation of fracture f1 is depicted by a horizontal line. The water level in the flooded drainage ditch shown in Plate 1 is provided to illustrate the interpreted boundary condition. The curves designate steady state solutions expected for fully penetrating wells under confined and unconfined conditions. Since the majority of monitoring locations are not fully penetrating and this is not a homogeneous porous aquifer, it is not expected that the curves should fit the data. The water level data suggest a drained radius for fracture f1 of between 6 and 16 m.

plitude strength and reflector arrival times. Furthermore, differences in weather (precipitation and temperature), different GPR systems, and different wave field orientation result in additional sources of amplitude differences between our 2-D and 3-D surveys. Thus we compare the relative changes (or lack of changes) observed along each horizontal reflector within a survey. GPR surveys acquired under identical conditions (acquisition parameters, weather, short time lapse, and equipment) should allow more quantitative comparison of surveys conducted before and during pumping tests.

In analyzing shallow GPR reflectors, caution must be used in distinguishing the direct ground wave energy (transmitter to receiver) and possible system ringing that may be superimposed on the reflected energy. In the 0.5-m offset 2-D data the direct ground wave is received at 4.5 ns, and in the 1.5-m offset 3-D data the direct ground wave is received at 13.5 ns, whereas the reflector of interest is in the range of 24–30 ns. System ringing can be identified by comparing data collected at varying antenna offsets and/or correlating reflection data to CMP reflectors with hyperbolic moveout. At Bissen Quarry both techniques were employed, and no ringing was observed in the GPR data even at the small 0.5-m antenna offset.

The vertical resolution of radar data must be examined when determining the GPR signal response for thin layers. Radar surveys collected in geologic formations with depth-imaging objectives of the order of meters commonly employ frequencies of 50–200 MHz with a corresponding vertical resolution of approximately 1 m to 25 cm. Fracture apertures are highly variable, and for most geologic environments, except perhaps karst, the apertures are orders of magnitude less than radar resolution. EM theory predicts that thin layers (subresolution thickness) are capable of introducing detectable changes in radar data [*Straton*, 1941; *Tsoflias*, 1999]. For the simplified case of a plane wave normal incident to a layer, signal changes are a function of the reflectivity of media, layer thickness, and signal frequency. Finite difference modeling of the response of a 100-MHz signal to a 1-cm layer produced similar behavior to the 200-MHz and 2-cm layer model of Figure 7 but with reduced magnitude of amplitude changes because of reduction of layer thickness and signal frequency. Close inspection of the 200-MHz model traces of Figure 7 show that the apparent time delay of the drained waveform is actually a very small positive amplitude deflection, whereas the saturated model trace onset is a large negative deflection. The reverse polarity of the saturated versus drained waveforms is what is expected from the dielectric constant contrasts between dolomite (8), water (80), and air (1). Also, the stretched waveform of the drained fracture is a result of the low-reflective interface compared to the saturated fracture interface. Although detailed review, modeling, and analysis of thin layer theory is beyond the scope of this study, we have demonstrated that subresolution thickness layer response can be correlated to physical properties and interpreted with confidence in GPR data. Such analyses are well suited to hydrologic studies because the large dielectric constant of water introduces detectable dielectric contrasts in geologic formations.

Hydrogeologic data supporting the GPR interpretation are not ideal, as expected for a fractured aquifer. In such aquifers, piezometers should ideally monitor isolated fractures or high-permeability zones to determine their response. However, in general, water level data support the interpretation from the GPR data. The pumping test data, not unexpectedly, do not yield a simple steady state response that is precisely correlated to the change in GPR amplitude. An alternative approach to provide support for the GPR interpretation would be to monitor fracture f1 by installing several piezometers in fracture f1 around the pumping well at varying orientations and distances. This would require installation of three or more additional piezometers if a priori knowledge about the draining radius of the fracture were available. We do not consider this method practical. The degree of hydrologic monitoring required to obtain the equivalent information that was obtained by noninvasive GPR techniques demonstrates the strength of this method. GPR is not proposed as a stand-alone tool for characterizing the hydraulic properties of fractures, but GPR data, combined with hydrological data, can yield insights not available from other methods. The ability to observe hydraulic boundaries and partially saturated conditions with a noninvasive technique are the major strengths of this method.

## 6. Conclusions

Ground-penetrating radar was successfully employed for three-dimensional, real-time monitoring of a pumping test in a fractured medium. Forward modeling of radar response to varying fracture saturation identified distinct differences in signal waveform between saturated and unsaturated conditions in fractures. GPR surveys taken before and during a pumping test recorded the signal expected for these conditions, and the GPR surveys are confirmed with head measurements in piezometers. In addition, GPR profiles provided information about hydrologic boundaries, despite adverse weather conditions that limited the usefulness of pumping test data. This study demonstrates that GPR surveying combined with hydraulic data can provide improved understanding of fractured formation fluid flow properties on the well scale.

**Acknowledgments.** We would like to thank Maureen Muldoon, Kenneth Bradbury, the staff at WGNHS, the Peninsular Agricultural Research Station, and Ivan Bissen. We would also like to thank William Clement and anonymous reviewers for their comments which improved the manuscript. Computing support was provided by The University of Texas Institute for Geophysics. This work was funded by a Geological Society of America Student Research Award, the W.R. Muehlberger Field Geology Scholarship Fund, the Gulf Coast Association of Geological Societies, the Owen-Coates Fund of the Geology Foundation of the University of Texas at Austin, and a National Science Foundation Traineeship in Hydrology (NSF grant GER-9454098).

## References

Beres, M., Jr., and F. P. Haeni, Application of ground penetrating radar methods in hydrogeologic studies, *Ground Water*, *29*, 375–386, 1991.

Birken, R., and R. Versteeg, Use of four dimensional GPR and advanced visualization methods to determine subsurface fluid flow, in *Seventh International Conference on Ground Penetrating Radar*, vol. *1*, pp. 377–381, Univ. of Kans., Lawrence, 1998.

Bradbury, K. R., and M. A. Muldoon, Hydrogeology and groundwater monitoring of fractured dolomite in the Upper Door Priority Watershed, Door County, Wisconsin, *Open File Rep.*, *WOFR 92-2*, Wis. Geol. Nat. Hist. Surv., Madison, 1992.

Brewster, M. L., and A. P. Annan, Ground-penetrating radar monitoring of a controlled DNAPL release: 200 MHz radar, *Geophysics*, *59*, 1211–1221, 1994.

Davis, J. L., and A. P. Annan, Ground penetrating radar for high-resolution mapping of soil and rock stratigraphy, *Geophys. Prospect.*, *37*, 531–551, 1989.

Dubois, J. C., Borehole radar experiment in limestone: Analysis and data processing, *First Break*, *13*, 57–67, 1995.

Endres, A. L., D. L. Rudolph, and W. P. Clement, Monitoring of a pumping test in an unconfined aquifer with ground penetrating radar, in *Symposium on the Application of Geophysics to Engineering and Environmental Problems*, vol. 1, pp. 483–492, Environ. and Eng. Geophys. Soc., Reno, Nev., 1997.

Endres, A. L., W. P. Clement, and D. L. Rudolph, Ground penetrating radar imaging of an aquifer during a pumping test, *Ground Water*, in press, 2000.

Fetter, C. W., *Applied Hydrogeology*, 3rd ed., Macmillan, Indianapolis, Indiana, 1994.

Geier, J., W. S. Dershowitz, P. C. Wallmann, and T. W. Doe, Discrete fracture modelling of in-situ hydraulic and tracer experiments, in *Fractured and Jointed Rock Masses*, pp. 511–518, A. A. Balkema, Brookfield, Vt., 1995.

Greaves, R. J., D. P. Lesmes, J. M. Lee, and M. N. Toksoz, Velocity variations and water content estimated from multi-offset, ground penetrating radar, *Geophysics*, *61*, 683–695, 1996.

Mellett, J. S., Ground penetrating radar applications in engineering, environmental management, and geology, *J. Appl. Geophys.*, *33*, 157–166, 1995.

Muldoon, M. A., and K. R. Bradbury, Hydrogeology of the fractured Silurian dolomite aquifer, Door County, Wisconsin in *The Silurian Dolomite Aquifer of the Door Peninsula: Facies, Sequence Stratigraphy, Porosity and Hydrogeology: Fieldtrip Guidebook for 1996 Fall Field Conference of the Great Lakes Section of the SEPM*, pp. 26–124, Soc. for Sediment Geol., Tulsa, Okla., 1996.

Muldoon, M. A., and K. R. Bradbury, Tracer study for characterization of groundwater movement and contaminant transport in fractured dolomite, *Final Rep.*, *WOFR 98-2*, Wis. Geol. Nat. Hist. Surv., Madison, 1998.

Neuman, S. P., Analysis of pumping test data from anisotropic unconfined aquifers considering delayed gravity response, *Water Resour. Res.*, *11*, 329–342, 1975.

Poot, H., 2D finite difference time domain modeling for GPR, Rep. *TA/TG 98.06 CTG/TG 98.05*, Delft, Univ. of Technol., Delft, Netherlands, 1998.

Straton, J., A., *Electromagnetic Theory*, McGraw-Hill, New York, 1941.

Taner, M. T., and F. Koehler, Velocity spectra-digital computer derivation and applications of velocity functions, *Geophysics*, *39*, 859–881, 1969.

Thiem, G., *Hydrologische Methoden*, Gebhardt, Leipzig. Germany, 1906.

Tsoflias, G. P., and J. M. Sharp, Three-dimensional hydrogeologic characterization of fractured carbonate aquifers using ground-penetrating radar, Trans. *Gulf Coast Assoc. Geol. Soc.*, *XL*(VIII), 439–447, 1998.

Tsoflias, G. P., Hydrogeologic characterization of fractured carbonate aquifers employing ground-penetrating radar, Ph.D. thesis, Univ. of Tex. at Austin, 1999.

van Overmeeren, R. A., GPR and wetlands in the Netherlands, in *Seventh International Conference on Ground Penetrating Radar*, vol. 1, *251–256*, Univ. of Kans., Lawrence, 1998.

T. Halihan, School of Geology, Oklahoma State University, Stillwater, OK 74078.

J. M. Sharp Jr., Department of Geological Sciences, University of Texas at Austin, Mail Code C1101, Austin, TX 78712. (jmsharp@mail.utexas.edu)

G. P. Tsoflias, Minerals Management Service, U.S. Department of the Interior, 1201 Elmwood Park Blvd., New Orleans, LA 70123. (George.Tsoflias@mms.gov)

(Received October 18, 1999; revised August 31, 2000;
accepted September 21, 2000.)